Actin Mutations in Dilated Cardiomyopathy, a Heritable Form of Heart Failure

Timothy M. Olson,* Virginia V. Michels, Stephen N. Thibodeau, Yin-Shan Tai, Mark T. Keating

To test the hypothesis that actin dysfunction leads to heart failure, patients with hereditary idiopathic dilated cardiomyopathy (IDC) were examined for mutations in the cardiac actin gene (*ACTC*). Missense mutations in *ACTC* that cosegregate with IDC were identified in two unrelated families. Both mutations affect universally conserved amino acids in domains of actin that attach to Z bands and intercalated discs. Coupled with previous data showing that dystrophin mutations also cause dilated cardiomyopathy, these results raise the possibility that defective transmission of force in cardiac myocytes is a mechanism underlying heart failure.

Heart failure is a major medical problem that affects 700,000 individuals per year in the United States and accounts for annual costs of $10 to $40 billion (*1*). Heart failure is the primary manifestation of dilated cardiomyopathy, a group of disorders characterized by cardiac dilation and pump dysfunction. Half of patients with dilated cardiomyopathy are diagnosed with idiopathic dilated cardiomyopathy (IDC), isolated heart failure of unknown etiology (affecting 5 to 8 in 100,000 individuals) (*2*). Cardiac transplantation is the only definitive treatment for end-stage disease.

IDC is hereditary in at least 20% of cases (*3*), indicating that genetic factors are important in its pathogenesis. In both familial and nonfamilial IDC, disease onset is delayed (mean age at diagnosis = 45 ± 17 years), and the 5-year mortality rate is 50% after symptoms develop (*3*, *4*). Consequently, few multigeneration IDC families with many affected, living individuals have been identified. Although chromosomal loci for IDC (1p1-q1, 1q32, 3p22-p25, 9q13-q22, and 10q21-q23) have been identified by genetic linkage analysis in rare families (*5*), these families are too small for positional cloning of IDC genes. Furthermore, these loci do not identify all potential candidate genes, like cardiac actin (*ACTC*) on chromosome 15q14. As an alternative strategy, we used a candidate gene approach in small IDC families.

T. M. Olson and Y.-S. Tai, Department of Pediatrics, Division of Cardiology, University of Utah Health Sciences Center, Salt Lake City, UT 84112, USA.
V. V. Michels, Department of Medical Genetics, Mayo Clinic/Foundation, Rochester, MN 55905, USA.
S. N. Thibodeau, Department of Laboratory Medicine and Pathology, Mayo Clinic/Foundation, Rochester, MN 55905, USA.
M. T. Keating, Howard Hughes Medical Institute, Eccles Institute of Human Genetics, Department of Human Genetics, and Department of Medicine, University of Utah Health Sciences Center, Salt Lake City, UT 84112, USA.
*To whom correspondence should be addressed. E-mail: timo@howard.genetics.utah.edu

We studied two unrelated families with autosomal dominant IDC, one of German ancestry and the other of Swedish-Norwegian ancestry (Fig. 1). Families were phenotypically characterized by echocardiography (*3*, *6*). IDC was defined as left ventricular (LV) end-diastolic dimension >95th percentile for age and body surface area, and shortening fraction < 28% (*7*). The results of phenotypic evaluation are shown in Table 1. Individuals in both families had variable age at diagnosis (1 to 41 years), similar to other IDC families, with age at diagnosis differing by as much as 20 to 50 years (*5*, *8*). Heart biopsy specimens from the proband of each family revealed histopathologic findings consistent with IDC (Fig. 2). Neither family had phenotypic features of hypertrophic cardiomyopathy (*9*).

Actin is essential for normal structure and function of cardiac myocytes. During development, five of the six actin isoforms encoded by separate genes are expressed in myocytes. In mature cardiac myocytes, however, only cardiac and skeletal actin are expressed, and cardiac actin is the major isoform (~80%) (*10*, *11*). To test the hypothesis that actin dysfunction leads to heart failure, we investigated the cardiac actin gene (*ACTC*) on chromosome 15q14 as a candidate for IDC. Oligonucleotide primers complementary to flanking intron sequence were developed for the six exons of *ACTC* (*12*), and single-strand conformation polymorphism (SSCP) analyses (*13*) were performed.

SSCP analyses of *ACTC* in kindred 1453 (K-1453) identified an anomalous conformer for exon 5 that cosegregated with IDC (*14*). Sequencing (*15*) of the conformer revealed a G-to-A substitution in codon 312 (Arg312His) (Fig. 1A). We confirmed this alteration by testing for a new Bcl I restriction site. It was inherited by three individuals with IDC (ages 36, 5, and 2) and a 15-year-old who has not developed IDC.

Analysis of kindred 9695 (K-9695) revealed an anomalous conformer for *ACTC* exon 6 that cosegregated with IDC (Fig. 1B). DNA sequence analysis demonstrated an A-to-G substitution in codon 361 (Glu361Gly). This alteration was inherited by two individuals with IDC (ages 41 and 14) in addition to a 34-year-old with a

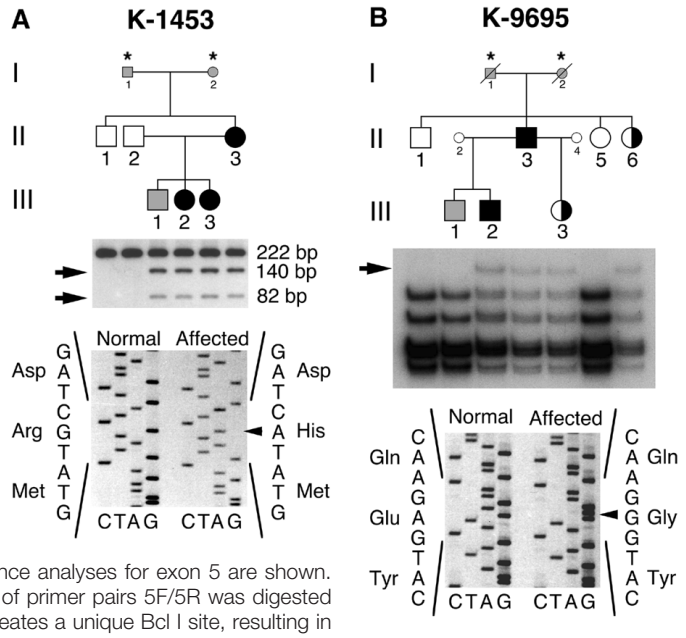

Fig. 1. *ACTC* missense mutations in two IDC families. Pedigree symbols designate the following traits: circles, females; squares, males; diagonal lines, deceased; filled, IDC; half-filled, LV dilation or borderline LV size; empty, normal; shaded, uncertain; *, insufficient data because of death (I.1 and I.2, K-9695), preexisting ischemic heart disease (I.1, K-1453), or refusal to participate (I.2, K-1453). Spouses were classified as normal. (**A**) Below K-1453, the results of PCR-RFLP (restriction fragment length polymorphism) and sequence analyses for exon 5 are shown. The 222-bp PCR product of primer pairs 5F/5R was digested with Bcl I. The mutation creates a unique Bcl I site, resulting in 140- and 82-bp fragments (arrows) that cosegregate with IDC. Sequence analysis reveals a G-to-A point mutation, resulting in a conservative arginine-to-histidine substitution. (**B**) Below K-9695, the results of SSCP and sequence analyses for exon 6 are shown. The anomalous conformer (arrow) cosegregates with IDC. Sequence analysis reveals an A-to-G point mutation, resulting in a nonconservative glutamic acid–to–glycine substitution.

dilated heart and a 9-year-old with borderline heart size.

To eliminate the possibility that these substitutions were polymorphisms within the normal population, we tested 435 unrelated control individuals (870 chromosomes). No anomalous SSCP conformers were identified for *ACTC* exons 5 and 6 in these controls. In addition, sequence comparisons revealed that both substitutions affect amino acids that are invariant in all human actin isoforms and actin in mice, *Drosophila*, yeast, and rice (*14*, *16*). Arg312His and Glu361Gly substitutions have not been evaluated in functional studies of mutant actin. However, an Arg312Ala substitution causes reduced viability of haploid yeast (*17*). Thus, the *ACTC* variants described here are likely to be IDC-associated mutations rather than rare polymorphisms.

ACTC is one of six actin genes in humans (*18*), none of which thus far have been implicated in human disease. In cardiac myocytes, cardiac actin is the main component of the thin filament of the sarcomere. One end of the polarized actin filament forms cross-bridges with myosin, and the other end is immobilized, attached to a Z band or an intercalated disc (*11*, *19*). Thus, actin transmits force between adjacent sarcomeres and neighboring myocytes to effect coordinated contraction of the heart. The mutations we identified occur in subdomains 1 and 3 of the actin monomer (Fig. 3), which form the immobilized end of the actin filament. Moreover, the Glu361Gly substitution is within a common binding domain for actinin, a protein comprising Z bands and intercalated discs, and dystrophin, a protein linking myofibrils to the extracellular matrix (*20*).

In addition to our data, several lines of evidence support the hypothesis that relatively subtle molecular defects in force-transmitting proteins, like actin, lead to myocyte dysfunction and heart failure. First, missense mutations throughout the actin gene in *Drosophila* result in abnormal structure and function of flight muscle (*17*). Second, transgenic expression of a noncardiac actin in cardiac actin–deficient mice causes heart enlargement and dysfunction, resembling human IDC (*21*). Third, missense mutations in dystrophin have been identified in X-linked dilated cardiomyopathy (*22*). In mice, heterozygous disruption of *ACTC* is not associated with heart abnormalities (*21*). Thus, the missense mutations in *ACTC* defined here likely lead to altered actin function rather than loss of function.

Hypertrophic cardiomyopathy (HCM) is characterized by hypertrophy of the heart, in contrast to IDC, which leads to chamber dilation and heart failure. The genes implicated in HCM all encode proteins involved in generation of force (β-myosin heavy chain, cardiac troponin T, α-tropomyosin, myosin-binding protein C, and essential and regulatory myosin light chains) (*23*). This has led to the hypothesis that HCM is caused by chronic reduction of force generation, which stimulates secondary myocyte hypertrophy (*24*). The cellular mechanism underlying IDC, however, may not involve force generation. Actin provides a scaffold for force generation by interacting with myosin, but the mutations we identified are not in regions that interact with myosin (*25*). Instead of generating force, actin transmits force to adjacent sarcomeres and myocytes and, like dystrophin, transmits force to the extracellular matrix. Further evidence that IDC does not result from a primary defect in force generation is that pathologic features of HCM are not observed during the course of IDC. We propose that IDC results from an episodic defect in force transmission. This defect may predispose affected myocytes to mechanical injury and cumulative cell death, secondary interstitial fibrosis, and cardiac dilation, a degenerative process that may take decades to develop.

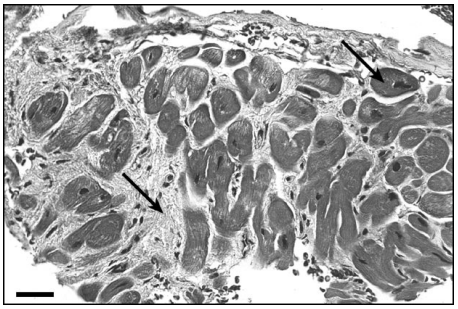

Fig. 2. Photomicrograph from right ventricle biopsy specimen of individual II.3 in K-9695 demonstrates moderate focal interstitial fibrosis (left arrow) and myocyte hypertrophy (right arrow). There is no evidence of myofibrillar disarray, as seen in hypertrophic cardiomyopathy, or myocarditis. Histopathologic findings were similar but less severe for individual II.3 in K-1453 (*14*). The specimen was stained with hematoxylin and eosin. Bar, 50 μM.

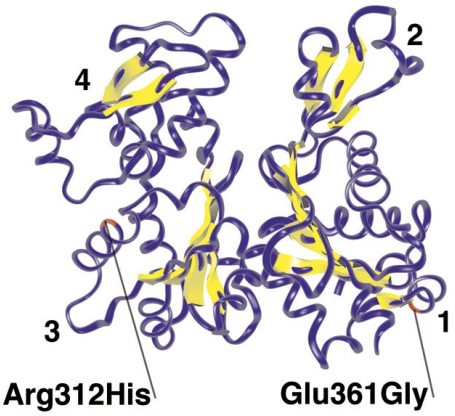

Fig. 3. Schematic representation of the cardiac actin monomer and location of IDC-associated mutations. The figure is based on the x-ray crystallographic structure of actin (*27*). The four structural subdomains are indicated.

Table 1. Phenotypic data for IDC families with missense mutations in *ACTC*. The 95th percentiles for LV end-diastolic dimension, based on body surface area and age, are indicated in parentheses. Normal shortening fraction is ≥28%. Abnormal values are indicated in bold type. Individuals <20 years of age with normal values were classified as uncertain, on the basis of ~5 to 10% disease penetrance in this age group (*26*). Phenotypic data were obtained before DNA analyses. BSA, body surface area; LV, left ventricle.

Pedigree	Age (years)	BSA (m^2)	LV end-diastolic dimension (mm)	Shortening fraction (%)	Phenotypic assignment	Cardiac actin genotype
			K-1453			
II.1	39	1.96	51 (54)	35	Normal	Normal
II.3	36	1.53	**59** (49)	**20**	IDC	Arg312His
III.1	15	1.84	53 (54)	36	Uncertain	Arg312His
III.2	5	0.74	**48** (38)	**13**	IDC	Arg312His
III.3	2	0.62	**37** (35)	**27**	IDC	Arg312His
			K-9695			
II.1	42	1.81	51 (52)	35	Normal	Normal
II.3	41	1.85	**58** (53)	**7**	IDC	Glu361Gly
II.5	38	1.65	49 (51)	43	Normal	Normal
II.6	34	1.54	**51** (49)	31	LV dilation	Glu361Gly
III.2	16	1.61	45 (51)	38	Uncertain	Normal
III.3	14	1.38	**51** (48)	**22**	IDC	Glu361Gly
III.1	9	1.05	43 (43)	37	Borderline LV dilation	Glu361Gly

REFERENCES AND NOTES

1. W. T. Abraham and M. R. Bristow, *Circulation* **96**, 2755 (1997).
2. T. A. Manolio *et al*., *Am. J. Cardiol.* **69**, 1458 (1992); E. K. Kasper *et al*., *J. Am. Coll. Cardiol.* **23**, 586 (1994).
3. V. V. Michels *et al*., *N. Engl. J. Med.* **326**, 77 (1992).
4. G. W. Dec and V. Fuster, *ibid.* **331**, 1564 (1994).
5. *Mendelian Inheritance in Man* 115200, 600884,

601154, 601493, and 601494; T. M. Olson and M. T. Keating, *Trends Cardiovasc. Med.* **7**, 60 (1997); K. R. Bowles *et al.*, *J. Clin. Invest.* **98**, 1355 (1996).
6. Echocardiograms and blood samples for DNA analyses were obtained from participating family members after informed, written consent.
7. The following formulas were used: body surface area (BSA) (m^2) = 0.007184 × height (cm)$^{0.725}$ × weight (kg)$^{0.425}$ [D. Du Bois and E. F. Du Bois, *Arch. Intern. Med.* **17**, 863 (1916)]; 95th percentile for LV end-diastolic dimension (mm) = 45.3 (BSA)$^{1/3}$ − 0.03 (age) − 7.2 + 12% [W. L. Henry, J. M. Gardin, J. H. Ware, *Circulation* **62**, 1054 (1980)]; shortening fraction (%) = 100 × (LV end-diastolic dimension − LV end-systolic dimension) ÷ LV end-diastolic dimension.
8. V. V. Michels, D. J. Driscoll, F. A. Miller, *Am. J. Cardiol.* **55**, 1232 (1985); T. M. Olson and M. T. Keating, *J. Clin. Invest.* **97**, 528 (1996).
9. Hypertrophy of the heart was not evident on electrocardiograms or echocardiograms. Myofibrillar disarray, which is characteristic of hypertrophic cardiomyopathy, was absent on histopathologic examination of cardiac biopsy specimens.
10. I. R. Herman, *Curr. Opin. Cell Biol.* **5**, 48 (1993); M. Gimona, *et al.*, *Cell Motil. Cytoskel.* **27**, 108 (1994); J. Vandekerckhove, G. Bugaisky, M. Buckingham, *J. Biol. Chem.* **261**, 1838 (1986).
11. M.-H. Lu *et al.*, *J. Cell Biol.* **117**, 1007 (1992);
12. Primers were designed according to the published genomic DNA sequence for *ACTC* [H. Hamada, M. G. Petrino, T. Kakunaga, *Proc. Natl. Acad. Sci. U.S.A.* **79**, 5901 (1982)] and OLIGO 4.03 Primer Analysis Software (National Biosciences, Plymouth, MN). The forward primer for exon 5 overlaps 5 base pairs (bp) of coding sequence to avoid a repetitive dinucleotide sequence near the intron-exon boundary. Primer sequences are as follows: exon1F, 5′-CCCCTGAAGCTGTGCCAAGA-3′; exon1R, 5′-GGCTCGGCGGGAAGTTTAC-3′; exon2F, 5′-TAAATGGACAAGACACTGATTAT-3′; exon2R, 5′-CAGCAAGGTCGGTGACTT-3′; exon3F, 5′-GCTAGAGCAGTGGTGTTGTC-3′; exon3R, 5′-AG-GTAGGCGGATTCAGTG-3′; exon4F, 5′-CTCACTGA-ATCCGCCTACCT-3′; exon4R, 5′-CTACACCAGACC-CTACAACTC-3′; exon5F, 5′-GACTCGTTCCCAGGT-ATG-3′; exon5R, 5′-GATCTCCCACTCACAAAAG-3′; exon 6F, 5′-AAGTTTTTGTTTTCTTCTGC-3′; exon 6R, 5′-CATAATACCGTCATCCTGA-3′. Polymerase chain reaction (PCR) product sizes for exons 1 to 6 are 167, 457, 292, 291, 222, and 214 bp, respectively.
13. M. Orita, H. Iwahana, H. Kanazawa, T. Sekiya, *Proc. Natl. Acad. Sci. U.S.A.* **86**, 2766 (1989). PCR was performed with 25 ng of genomic DNA, 10 mM tris-HCL (pH 8.3), 50 mM KCl, 1.5 mM $MgCl_2$, 200 μM deoxyguanosine triphosphate, 200 μM deoxyadenosine triphosphate, 200 μM deoxythymidine triphosphate, 200 μM deoxycytidine triphosphate (dCTP), 0.5 μM forward primer, 0.5 μM reverse primer, 10% glycerol, 0.05 U Taq DNA polymerase, and 1 μCi of [α-^{32}P]dCTP in a final volume of 10 μl. Amplification conditions were 94°C for 5 min, followed by 30 cycles of 94°C for 30 s, 52° to 60°C for 30 s, and 72°C for 30 s followed by 72°C for 10 min (Perkin-Elmer Cetus 9600 thermocycler). For exon 2, 10 μl of PCR product was digested with Bgl II, resulting in 198- and 259-bp fragments. Reactions were diluted with 25 μl of 0.1% SDS, 10 mM EDTA, and 25 μl of 95% formamide dye. Diluted samples were denatured at 94°C for 10 min, and 3-μl samples were subjected to gel electrophoresis under three conditions: 0.5× and 1× Mutation Detection Enhancement gels (FMC Bioproducts, Rockland, ME) at 800 V for 14 to 30 hours (room temperature) and 10% nondenaturing polyacrylamide (49:1 polyacrylamide:bisacrylamide) with 10% glycerol at 30 W for 4 to 6 hours (4°C). Gels were then dried for autoradiography.
14. T. M. Olson *et al.*, data not shown.
15. Normal and anomalous single-strand conformers were cut from dried gels and eluted in 100 μl of water at 65°C for 30 min. The eluted DNA (10 μl) was used as a template for a second PCR with the original primer pair. Products were fractionated in 1% agarose gels and DNA was purified by phenol and chloroform extraction. Forward and reverse [α-^{33}P]-ddNTP (dideoxynucleoside triphosphates) cycle sequencing was performed with a Thermo Sequenase kit (Amersham Life Sciences, Cleveland, OH). Mutations were confirmed by PCR amplification and cycle sequencing of genomic DNA. No additional mutations were identified in other exons of ACTC for either family.
16. Comparison of actin sequences was made by use of the combined protein database and the NCBI BLAST Web site (http://www.ncbi.nlm.nih.gov/cgi-bin/BLAST/nph-blast?form=1).
17. E. S. Hennessey, D. R. Drummond, J. C. Sparrow, *Biochem. J.* **282**, 657 (1993).
18. *Mendelian Inheritance in Man* 102540.
19. K. C. Holmes, D. Popp, W. Gebhard, W. Kabsch, *Nature* **347**, 44 (1990); C. C. Gregorio, *Cell Struct. Funct.* **22**, 191 (1997).
20. B. A. Levine, A. J. G. Moir, V. B. Patchell, S. V. Perry, *FEBS Lett.* **298**, 44 (1992); P. A. Kuhlman, L. Hemmings, D. R. Critchley, *ibid.* **304**, 201 (1992).
21. A. Kumar *et al.*, *Proc. Natl. Acad. Sci. U.S.A.* **94**, 4406 (1997).
22. *Mendelian Inheritance in Man* 302045; R. Oritz-Lopez, H. Li, J. Su, V. Goytia, J. A. Towbin, *Circulation* **95**, 2434 (1997).
23. P. Spirito, C. E. Seidman, W. J. McKenna, B. J. Maron, *N. Engl. J. Med.* **336**, 775 (1997).
24. E. B. Lankford, N. D. Epstein, L. Fananapazir, H. L. Sweeney, *J. Clin. Invest.* **95**, 1409 (1995); H. Watkins, C. E. Seidman, J. G. Seidman, H. S. Feng, H. L. Sweeney, *ibid.* **98**, 2456 (1996).
25. E. Reisler, *Curr. Opin. Cell Biol.* **5**, 41 (1993).
26. L. Mestroni *et al.*, *Br. Heart J.* **72**, S35 (1994).
27. W. Kabsch, H. G. Mannherz, D. Suck, E. F. Pai, K. C. Holmes, *Nature* **347**, 37 (1990). The Insight II molecular modeling system software program (Biosym Technologies, San Diego) was used to create Fig. 3.
28. We thank D. Schaid, F. Miller, D. Driscoll, G. Orsmond, R. Shaddy, and H. Holtzer for support and helpful discussions; W. Edwards (print for Fig. 2); and J. Ross, D. Renlund, J. Mason, J. Anderson, M. Karst, and N. Kishimoto for assistance. Supported by Clinician Scientist Award 96004630 from the American Heart Association (T.M.O.), NIH SCOR grant 5-P50-HL-53773, Project 6 (M.T.K.), the John Patrick Albright Foundation, Public Health Services Research Grant M01-RR00064 from the National Center for Research Resources, and the Technology Access Section of the Utah Genome Center.

3 October 1997; accepted 9 March 1998

Ribonuclease P Protein Structure: Evolutionary Origins in the Translational Apparatus

Travis Stams, S. Niranjanakumari, Carol A. Fierke, David W. Christianson*

The crystal structure of *Bacillus subtilis* ribonuclease P protein is reported at 2.6 angstroms resolution. This protein binds to ribonuclease P RNA to form a ribonucleoprotein holoenzyme with optimal catalytic activity. Mutagenesis and biochemical data indicate that an unusual left-handed βαβ crossover connection and a large central cleft in the protein form conserved RNA binding sites; a metal binding loop may comprise a third RNA binding site. The unusual topology is partly shared with ribosomal protein S5 and the ribosomal translocase elongation factor G, which suggests evolution from a common RNA binding ancestor in the primordial translational apparatus.

Bacterial ribonuclease P (RNase P) is composed of two subunits, an RNA of about 400 nucleotides and a protein of about 120 residues, and the ribonucleoprotein holoenzyme plays a critical supporting role for the translational apparatus by catalyzing the 5′ maturation of pre-tRNA substrates (*1*). Absent the protein subunit, the RNA subunit (RNase P RNA) alone is catalytically active in the presence of elevated salt concentrations and was one of the first ribozymes discovered (*2*). However, the RNase P protein subunit is essential for physiological activity; it decreases the dependence of the reaction on Mg^{2+} concentrations (*2, 3*), it stabilizes the catalytically active conformation of the RNA subunit (*4*), and it enhances substrate affinity (*5*). The protein subunit also modulates substrate specificity (*6, 7*). For example, the protein subunit enhances processing of pre-4.5S RNA (*7*), an accessory molecule essential for ribosomal translocation (*8*).

The RNase P ribonucleoprotein holoenzyme (or the RNA subunit by itself) is very much like a classic protein enzyme in that substrate association is mediated by noncovalent interactions (*9*) and multiple turnovers are catalyzed (*2*). Catalysis requires divalent metal ions such as Mg^{2+} or Mn^{2+}, probably to provide nucleophilic metal-bound hydroxide ion for catalysis (*2, 10*); additionally, at least one metal ion stabilizes the hydrolytic transition state (*11*). Metal ions also stabilize RNA tertiary structure (*3, 12*) and binding of the pre-tRNA substrate (*11, 13*). Metal ions increase protein-RNA subunit affinity in the holoenzyme (*14*), but it is not known whether the protein subunit interacts directly with metals. It is interesting to consider that as the protein world evolved from the hypothetical RNA world, metal-dependent ribonucleoproteins such as the RNase P holoen-

T. Stams and D. W. Christianson, Roy and Diana Vagelos Laboratories, Department of Chemistry, University of Pennsylvania, Philadelphia, PA 19104–6323, USA.
S. Niranjanakumari and C. A. Fierke, Department of Biochemistry, Duke University Medical Center, Durham, NC 27710, USA.

*To whom correspondence should be addressed. E-mail: chris@xtal.chem.upenn.edu